# The Impact of Self-Phase Modulation on Digital Clock Recovery in Coherent Optical Communication

A. Serdar Tan[(1)], Henk Wymeersch[(1)], Pontus Johannisson[(2)], Martin Sjödin[(2)], Erik Agrell[(1)], Peter Andrekson[(2)], Magnus Karlsson[(2)]

[(1)] Communication Systems Group, Department of Signals and Systems, Chalmers University of Technology, SE-412 96 Göteborg, Sweden, ✉ ahmets@chalmers.se
[(2)] Photonics Laboratory, Department of Microtechnology and Nanoscience, Chalmers University of Technology, SE-412 96 Göteborg, Sweden

***Abstract*** *The impact of self-phase modulation on the estimation error variance of digital clock recovery schemes for coherent 16-QAM dual-polarization systems is investigated. The error variance increases severely compared to the linear case and the theoretical bounds.*

## Introduction

Nonlinear impairments create significant challenges in future M-QAM coherent systems at and beyond 100 Gbit/s[1]. The Kerr nonlinearity causes self-phase modulation (SPM) distorting the signal at high power levels. It may also affect the performance of the digital signal processing (DSP) algorithms in the receiver. Digital clock recovery is the first step in digital receiver with non-synchronous sampling since the signal must be resampled at the optimum sampling instant to reduce inter-symbol interference and the complexity of the subsequent blocks of the receiver. Notably, the impact of nonlinear impairments to digital clock recovery in coherent optical communications has received very little attention and existing studies do not consider the impact of SPM[2–4]. In this paper, we analyze the impact of SPM on practical feedback (FB) and feedforward (FF) digital clock recovery schemes based on the estimation error variance. We derive theoretical bounds on the estimation error variance and evaluate the increase of the error variance of practical estimators compared to the bounds and the linear case.

## System Model

We investigate a 112 Gbit/s 16-QAM dual polarization coherent optical communication system as given in Fig. 1. There are two independent data sequences transmitted through multiple amplifier stages with adjacent standard single-mode fiber (SMF) and dispersion-compensating fiber (DCF). The initial signal at the output of the transmitter (TX) is given by

$$\mathbf{r}_0(t) = \left[r_0^{(\mathrm{X})}(t)\ \ r_0^{(\mathrm{Y})}(t)\right]^{\mathrm{T}} = \sum_{n=1}^{N_d} \mathbf{A}_n \mathbf{p}(t-nT), \tag{1}$$

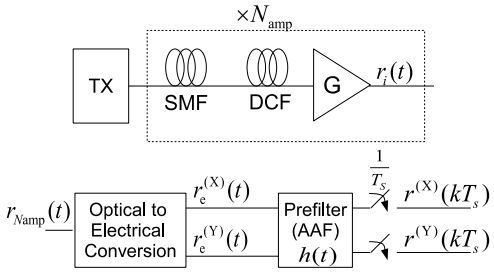


**Fig. 1**: Optical transmission and receiver model

where $\mathbf{A}_n = \mathrm{diag}\{a_n^{(\mathrm{X})}, a_n^{(\mathrm{Y})}\}$ is the $n^{th}$ data symbol matrix, $N_d$ is the number of data symbols, $T$ is the symbol duration, and $\mathbf{p}(t) = \sqrt{P_{\mathrm{in}}}\, p\,(t)\,[1\ 1]^{\mathrm{T}}$ is a pulse vector, in which $P_{\mathrm{in}}$ is a launch power, and $p(t)$ is a unit energy return-to-zero (RZ) pulse. We use two RZ optical pulses with 33% and 50% duty cycles[5],

$$p_{33}(t) = \frac{1}{\sqrt{E_{33}}} \sin\left(\frac{\pi}{2}\left[1+\sin\left(\frac{\pi t}{T}\right)\right]\right), \tag{2}$$

$$p_{50}(t) = \frac{1}{\sqrt{E_{50}}} \sin\left(\frac{\pi}{4}\left[1+\cos\left(\frac{2\pi t}{T}\right)\right]\right), \tag{3}$$

where $E_{33}$ and $E_{50}$ are energy normalization constants, and both pulses are time limited to $[-T/2, T/2]$. Then, ignoring the effect of SPM in the DCF due to the low input power, the optical signal after each amplifier is given by[6]

$$\mathbf{r}_i(t) = \mathbf{r}_{i-1}(t) \exp\left[j\gamma L_{\mathrm{eff}} \mathbf{r}_{i-1}^{\mathrm{H}}(t)\mathbf{r}_{i-1}(t)\right] + \mathbf{n}_i(t), \tag{4}$$

where $\gamma$ is the nonlinearity parameter of the SMF, and $L_{\mathrm{eff}} = \left(1-e^{-\alpha L}\right)/\alpha$ is the effective length of the SMF for attenuation $\alpha$ and length $L$. The noise due to amplified spontaneous emission (ASE) after each amplifier, $\mathbf{n}_i(t) = [n_i^{(\mathrm{X})}(t)\ n_i^{(\mathrm{Y})}(t)]^{\mathrm{T}}$, is modeled as a circularly symmetric complex Gaussian noise with variance

**Tab. 1**: System Parameter Values

| | | | |
|---|---|---|---|
| $\gamma_{\mathrm{smf}}$ | $1.2\ \mathrm{W^{-1}km^{-1}}$ | $D_{\mathrm{smf}}$ | $16.5\ \mathrm{ps/(nm\ km)}$ |
| $\alpha_{\mathrm{smf}}$ | $0.20\ \mathrm{dB/km}$ | $D_{\mathrm{dcf}}$ | $-120\ \mathrm{ps/(nm\ km)}$ |
| $\alpha_{\mathrm{dcf}}$ | $0.60\ \mathrm{dB/km}$ | $\lambda = c/\nu$ | $1.55\ \mu\mathrm{m}$ |
| $B$ | $14\ \mathrm{GHz}$ | $L_{\mathrm{smf}}$ | $80\ \mathrm{km}$ |
| $n_{\mathrm{sp}}$ | 1.5 | $N_{\mathrm{amp}}$ | 22 |

$\sigma^2 = h\nu n_{\mathrm{sp}} B(G-1)$, where $h$ is Planck's constant, $\nu$ is the optical frequency, $n_{\mathrm{sp}}$ is the spontaneous emission factor, $B$ is the bandwidth of the electrical filter at the receiver, and $G$ is the amplifier gain. The amplifiers compensate for the total attenuation in the SMF and DCF. The samples, $\mathbf{r}(kT_s)$, are obtained by sampling $[\mathbf{r}_{\mathrm{e}}(t) \otimes h(t)]$ (see Fig. 1) at $t = kT_s - \tau$, where $\tau$ is the timing offset between the transmitter and receiver clocks, $T_s = T/M,\ M \geq 2$, is the sampling period, $h(t)$ is the impulse response of the anti-aliasing filter (AAF), and $\otimes$ denotes convolution.

We ignore the effect of polarization mode dispersion to obtain feasible mathematical formulation under nonlinearity. We use the numerical values given in Tab. 1 for the system model.

### Digital Clock Recovery

We consider FB and FF clock recovery schemes to estimate $\tau$. FB recovery schemes require the generation of an error signal for each symbol, whereas FF schemes operate on blocks of samples. The FB and FF clock recovery diagrams are given in Figs. 2(a) and 2(b), respectively, where $\hat{\tau}$ is the timing offset estimate. The baud-rate output signal $\mathbf{y}(nT)$ is forwarded for further DSP.

We extend non-decision aided maximum likelihood based FF and FB estimators for single polarization[7] to cover dual-polarization. The FF timing estimation is extended by

$$\hat{\tau} = -\frac{T}{2\pi}\arg\left\{\sum_{k=0}^{MN_s-1}\left[\mathbf{r}(kT_s)\right]^{\mathrm{H}}\mathbf{z}(kT_s)e^{-j\pi k/M}\right\}, \tag{5}$$

where $N_s$ is the observation length in symbols, $\mathbf{z}(kT_s) = [e^{-j\pi k/M}\mathbf{r}(kT_s)] \otimes c(kT_s)$, and $C(f) = P\left(f - 1/2T\right)P^*\left(f + 1/2T\right)$, in which $P(f)$ is the spectrum of $p(t)$. Similarly, the error signal for FB timing estimation, i.e., the output of the timing error detector (TED), is extended by

$$\begin{aligned} e(n) =& \mathrm{Re}\left\{\mathbf{y}^{\mathrm{H}}(nT+\hat{\tau}_n)\left[\mathbf{y}(nT+T/2+\hat{\tau}_n)\right.\right. \\ &\left.\left.+\mathbf{y}(nT-T/2+\hat{\tau}_{n-1})\right]\right\}, \\ \hat{\tau}_{n+1} =& \hat{\tau}_n + \mu e(n), \end{aligned} \tag{6}$$

where $\mu$ is determined based on the loop bandwidth of the loop filter (see Fig. 2(a)).

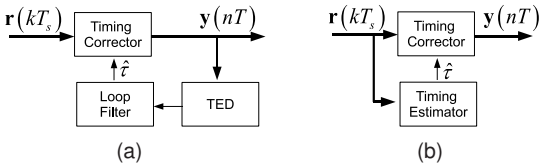


**Fig. 2**: Digital clock recovery blocks for (a) feedback, (b) feedforward schemes

**Tab. 2**: Simulation Parameters

| | |
|---|---|
| Baud Rate $(1/T)$ | 14 Gbaud |
| Sampling rate $(1/T_s)$ | $2.1/T = 29.4$ GHz |
| Simulation time | $10^6$ symbols |
| Loop bandw. for FB est. $(B_L)$ | $0.005/T = 70$ MHz |
| Block length for FF est. $(N_s)$ | 100 symbols |

### Bounds on Estimation Errors

The estimation error variance is a common tool to measure the estimator performance. Given a channel model, a theoretical lower bound on the error variance, namely the Cramér-Rao bound (CRB), can be calculated. The timing estimation error variance of any unbiased practical estimator is lower bounded as[8]

$$\mathbb{E}\left[(\tau-\hat{\tau})^2\right] \geq -\frac{1}{\mathbb{E}\left[\frac{\partial^2 \ln p(\mathbf{r}_s|\tau)}{\partial \tau^2}\right]} = -\frac{1}{J_{\tau\tau}}, \tag{7}$$

where $\mathbf{r}_s$ denotes the sequence of samples $\mathbf{r}(kT_s)$, $p\left(\mathbf{r}_s|\tau\right)$ is the probability density function of $\mathbf{r}_s$ given $\tau$, and $\mathbb{E}[\,\cdot\,]$ denotes expectation operation. A lower bound for the timing estimate variance based on the channel model in (4) after an AAF can be obtained by

$$J_{\tau\tau} = \frac{8T^2\pi^2}{\sigma^2 N_{\mathrm{amp}}}\sum_{n=1}^{N_s}\mathrm{tr}\left(\mathbf{A}_n^{\mathrm{H}}\mathbf{A}_n\right)\int_{-\frac{1}{T}}^{\frac{1}{T}} f^2\left|Q_n(f)\right|^2 \mathrm{d}f, \tag{8}$$

where $\mathrm{tr}(\cdot)$ is the trace operation on a matrix, and $Q_n(f)$ is the frequency spectrum of

$$q_n(t) = \left(g(t)e^{j\gamma L_{\mathrm{eff}} N_{\mathrm{amp}}\mathrm{tr}\left(\mathbf{A}_n^{\mathrm{H}}\mathbf{A}_n\right)|g(t)|^2}\right) \otimes h(t).$$

### Numerical Results

We demonstrate the impact of SPM for the model and simulation parameters given in Tabs. 1 and 2. In Figs. 3(a) and 3(b), the results for $p_{33}(t)$ are provided. Once $P_{\mathrm{in}}$ exceeds $-5$dBm, SPM starts to impact both the CRB and the practical estimator error variance, and as $P_{\mathrm{in}}$ exceeds 0dBm the increase in error variance compared to the linear case is severe. In Figs. 4(a) and 4(b), results are provided for $p_{50}(t)$, where the impact of SPM is similar to $p_{33}(t)$ for low to mid input powers. In the

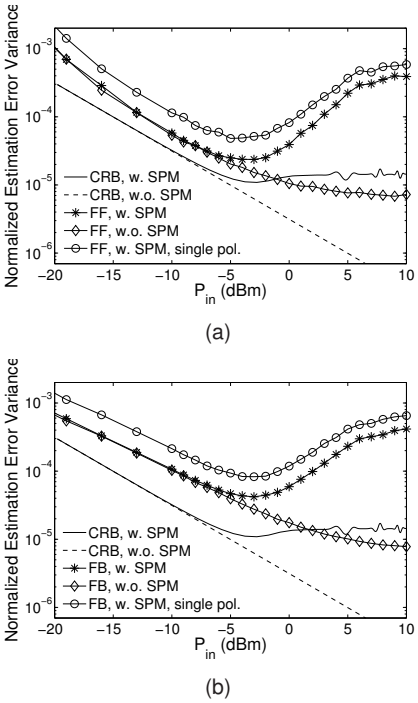


**Fig. 3**: The CRB and practical performance for 16-QAM for the pulse with 33% duty cycle. (a) FF; (b) FB

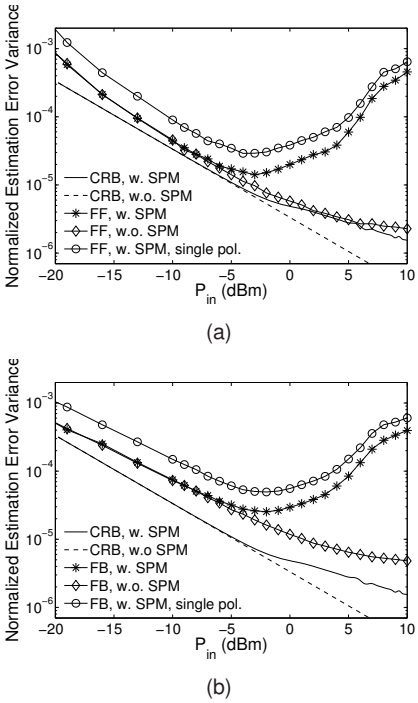


**Fig. 4**: The CRB and practical performance for 16-QAM for the pulse with 50% duty cycle. (a) FF; (b) FB

high input power regime, the CRB of $p_{50}(t)$ is significantly lower than that of $p_{33}(t)$. This is due to the fact that the pulse with lower duty cycle is affected more severely by the spectral broadening, and the AAF before the receiver removes a larger portion of the content of the signal. This difference exists in the practical estimators in the high input power regime as well, such that, at an input power of 5dBm, the variance of the FF estimator is around $6 \cdot 10^{-5}$ for $p_{50}(t)$, whereas it is $2 \cdot 10^{-4}$ for $p_{33}(t)$. In terms of error variance, for both FF and FB estimators, the optimal operation region is around $-$2dBm, at which point the variance of FB estimates is almost twice as large as that of FF estimates. Additionally, the figures demonstrate that the error variance is almost always halved when both polarizations are used for estimation.

The practical FF and FB timing estimates and the bounds turn out to be independent of the frequency offset, phase noise and polarization mixing, provided that these effects can be considered constant during an observation length. Further analysis (results not shown) revealed that the results for higher level QAM formats are quite similar to those of 16-QAM, given the same system model parameters. However, the practical estimation error variance curves and the CRB for QPSK systems are slightly lower than those of 16-QAM. Moreover, a unit increase in the number of amplifier stages shifts all curves leftwards and reduces the input power for optimal operation.

## Conclusions

This paper has studied the impact of SPM on clock recovery in coherent optical communication. We show that SPM has a strong impact on the timing estimation algorithms in terms of estimation error variance. The results reveal an optimal operation region, which we show to be $-$2dBm for the given system model. We also demonstrate that in the optimal region FF algorithms perform better than FB algorithms. Further, the gap between the estimation error variance and the theoretical bounds points to the potential of new estimation algorithms.


## Acknowledgement

We would like to acknowledge funding from VINNOVA within the IKT grant 2007-02930.


## References


1 G. Charlet et al., ECOC'06, OThC1 (2006).
2 T. Tanimura et al., ECOC'08, Mo3D2 (2008).
3 D. Zibar et al., ECOC'09, 7.3.4 (2009).
4 H. Louchet et al., ECOC'09, 7.3.5 (2009).
5 E. Ip et al., JLT, **24**, 1610 (2006).
6 K.P. Ho et al., JLT, **22**, 779 (2004).
7 U. Mengali et al., Synchronization Techniques for Digital Receivers, 428 (1997).
8 H.L. van Trees et al., Detection, Estimation, and Modulation Theory, 79 (1968).